JOURNAL OF GUIDANCE, CONTROL, AND DYNAMICS
Vol. 30, No. 2, March–April 2007

Scalable Sensing, Estimation, and Control Architecture for Large Spacecraft Formations

Terence H. McLoughlin* and Mark Campbell†
Cornell University, Ithaca, New York 14853

DOI: 10.2514/1.21322

A decentralized estimation architecture for large formations of spacecraft is introduced that, when coupled with a local controller, parameterizes the degree to which a node is a leader or a follower, eliminating the rigid classification of nodes as strictly leaders and followers. Measurements are provided by a single range/bearing sensor similar to the autonomous formation flying sensor. A reference point calculation is introduced that automatically compensates for noise in the estimation and sensing subsystems. A scheduling algorithm is developed that maximizes the information collected across the formation. The scheduling problem is posed as an infinite horizon optimization of either the formation information or covariance matrices, or the reference point information or covariance matrices. The resulting architecture is compared via simulation to a system in which each spacecraft has full knowledge of the fleet. Results show that performance degradation (root mean square position error and fuel usage) is very small compared to the ideal, full knowledge solution, and that the system performs better than the traditional leader–follower architecture.

Nomenclature

$\mathbf{C}_i$	=	measurement function Jacobian at spacecraft i
G_i	=	free virtual center weighting matrix at spacecraft i
g_i	=	free scalar virtual center weight at spacecraft i
$J_\infty^{(\cdot)}$	=	infinite horizon measurement scheduling cost
K	=	measurement period (dimensionless)
N	=	number of spacecraft
$\mathbf{Q}$	=	system process noise covariance relative to spacecraft i
$\mathbf{v}_i$	=	collection of measurement noise at spacecraft i
$\mathbf{w}_i$	=	system process noise disturbance relative to spacecraft i
x_{ci}	=	system virtual center state relative to spacecraft i
$\hat{x}_{ci}$	=	virtual center state estimate at spacecraft i
$\mathbf{x}_i$	=	system state relative to spacecraft i
$\hat{\mathbf{x}}_i$	=	system state estimate at spacecraft i
$\mathbf{Y}_{ci}$	=	information matrix of the virtual center state estimate at spacecraft i
$\mathbf{Y}_i$	=	information matrix of the system state estimate at spacecraft i
$\mathbf{Y}^p$	=	nominal steady-state periodic information matrix
$\mathbf{z}_i$	=	collection of system measurements at spacecraft i
λ_j	=	measurement duty to spacecraft j
$\bar{\boldsymbol{\mu}}_K$	=	periodic measurement sequence
$\boldsymbol{\mu}_\infty$	=	infinite horizon measurement schedule

I. Introduction

NASA is currently studying several large-scale spacecraft formation missions, many to be flown at the Earth–sun libration points. The location affords scientists a much clearer view of the universe, while also providing a convenient gravitational pull to be Earth following. The microarcsecond x-ray imaging mission (MAXIM) [1] is an x-ray interferometer composed of 33 spacecraft and will be able to image the event horizon of a black hole. The terrestrial planet finder (TPF) [2] mission shall enable scientists to find and study extra-solar planets similar to our own. Although several designs are currently under review, a TPF design by Lockheed Martin is composed of four, possibly six, free flying spacecraft which will function as an infrared interferometer. The stellar imager (SI) [3] mission postulates that stellar activity is key to understanding life in the universe. Specifically, SI is a large, space-based UV optical sparse aperture telescope/Fizeau interferometer designed to study the sun. The formation is designed to be flown at the Earth–sun libration point, as is TPF. The science of SI requires a large array of satellites in an irregular placement to accomplish its goals.

The combination of interferometry and large formations makes these and similar future missions especially challenging. Interferometry missions are especially challenging due to the high tolerance requirements. Such missions are currently slated to employ a multiple resolution control architecture: conventional thrusters and RF range and bearing sensors are to be used for coarse spacecraft control, and laser sensors and adaptive optics will provide fine optical path control [1,3]. The autonomous formation flying sensor (AFF) has been identified as a key component for coarse control of spacecraft formations [4,5]. The AFF provides range and bearing measurements between spacecraft based on global positioning system technology. Large formations of spacecraft present interesting challenges to the scientific community, including low fuel usage control for given precision requirements, fleet estimation given limited sensor and communication resources, and accurate relative state tracking to reduce fuel in the presence of the other challenges. Developing scalable algorithm tools is critical to the success of these missions.

Consider, as an example, the case of precision control to minimize fuel. Typical single spacecraft systems are allowed to drift with respect to an external frame, as it is not crucial (and would be fuel expensive) to reposition the satellite with respect to a model-based reference track. Multiple satellite missions can similarly relax the positioning of the formation in an external reference frame over small time horizons, but each individual spacecraft must control its relative position with respect to the fleet (and minimize fuel) for mission performance and safety [1–3]. Moreover, sensitivity of these factors grows with the number of spacecraft in the system. Further, although formations of two or three spacecraft can be designed with full relative sensing and communication to the fleet, affording an accurate estimate of all spacecraft in the fleet, formations of 16 or more spacecraft will certainly be constrained in the number of relative spacecraft measurements, as well as the number of communication links and available bandwidth. This, in turn, will

Presented as Paper 5022 at the AIAA Guidance, Navigation, and Control Conference and Exhibit, Providence, Rhode Island, 16–19 August 2004; received 22 November 2005; revision received 29 June 2006; accepted for publication 2 July 2006.

*Research Assistant; tmcloughlin@cornell.edu. Student Member AIAA.
†Associate Professor; mc288@cornell.edu. Senior Member AIAA.

have an effect on the system performance (relative position error and fuel usage) of each spacecraft in the formation.

The objective of this work is to develop a coordination architecture for future formations of spacecraft that is scalable in terms of integrated communication, sensing and estimation, and control. More specifically, under the constraints of a single range/bearing sensor, a relative control and estimation approach is developed that allows the formation as a whole to drift, thereby saving fuel, yet also attains very good relative positioning performance. Simulation results compared to the centralized solution show minimal degradation in terms of root mean square (rms) positioning error and fuel usage. In addition, results compare favorably to current leader–follower concepts. Information theory is used to develop a sensor scheduling scheme for the AFF sensor. Maximizing information, or maximizing knowledge of the formation both locally and within the cluster, is used to develop switching logic for the relative sensing subsystem. The resulting guidance, navigation, and control architecture can be considered to be *cyclic*, using the nomenclature introduced in the survey in [6].

In related work, the virtual center formation reference point algorithm was introduced in [7]. The algorithm is centralized based on the transmission of relative state estimates maintained across the fleet. The weights used are based on fuel reserve states, attempting to balance fuel usage across the fleet. The work in this paper includes a decentralized calculation of the virtual center, requiring very little communication. Also, the weights are based on the error covariance of the state estimates, leading to a system that compensates for increased noise in the estimation and sensing subsystems, due to such as spacecraft occlusions and hardware failures. The decentralized LQG architecture introduced in [8] produced semi-optimal performance for nonlinear plants and actuators using a communication architecture where all spacecraft communicate with one another. However, the resulting control law is suitable only for actuators that can produce unbounded inputs to the plant. The control used in this paper is a time-optimal controller for accurate formation keeping using binary on/off thrusters [9].

The sensor scheduling problem was first introduced in [10]. The paper contained several variations of the problem and algorithms for solving optimal sequences over short time horizons. The algorithm developed in [11] also produces an optimal schedule for short time horizons. A real time implementation of a sliding window is used, where only the first measurement of the optimal schedule is taken and the process is repeated at each time step. Optimality, however, is not guaranteed over long time horizons. Gupta et al. [12] finds an infinite horizon measurement scheme by choosing measurements at random; the probability of choosing each sensor is determined by solving a set of Riccati equations. The scheduling algorithm described in the sequel produces an optimal periodic infinite horizon measurement schedule that can be determined a priori. That the optimal infinite horizon measurement schedule is periodic was first proposed in [13]. The optimal schedule in [13] is determined by generating sequences at random.

The paper is outlined as follows: Sec. II details the general formation keeping problem in terms of the system dynamics, available measurements and associated estimator, controller, and also includes assumptions and notation used throughout. Section III describes the information weighted virtual center estimation algorithm and describes the leader–follower parameterization scheme. Section IV introduces the sensor scheduling problem and a solution and simple example are presented in Sec. V. Full simulation results are presented in Sec. VI followed by conclusions in Sec. VII.

II. Problem Statement

The formation control problem addressed in this work is motivated by SI-type missions and is formulated as follows: given a fleet of N spacecraft, each equipped with a single range/bearing sensor (RBS), find a sequence of measurements that adaptively maximizes, in some sense, knowledge of the fleet. Maximizing knowledge of the fleet directly benefits state error tracking, robustness, and collision avoidance, and, in Sec. VI, is shown to indirectly benefit performance in terms of lowering fuel usage. Several assumptions are made: 1) the range/bearing generates bearing measurements expressed in the inertial reference frame; 2) the RBS is omnidirectional, that is, it can provide range and bearing measurements with a full spherical field of view at any range; 3) acquisition of signal at the RBS is instantaneous and measurements within the nominal range/bearing performance specifications of the AFF sensor (2 cm, 1 arcsec) as described in [4] are provided instantaneously; 4) thrust maneuvers at each spacecraft are transmitted over a communication subsystem to all other spacecraft; 5) second order free-space dynamics govern the system. Assumption 1 is reasonable as future missions will necessarily be equipped with high resolution inertial attitude sensors for the optics subsystem. Attitude uncertainties can be incorporated into the RBS noise terms. Assumption 4 is reasonable as binary thrust commands can be transmitted over data links with very low bandwidth. Assumption 5 has been found to be accurate for deep space missions on a 0.5–1 day horizon [14,15]. The remaining assumptions shall be addressed at the end of the paper.

A. Spacecraft Dynamics

Each spacecraft is governed by second order dynamics; thus for N spacecraft, the discrete-time dynamics of the ith spacecraft, $\forall\ i \in \{1, \ldots, N\}$, are as follows;

$$x_i(k+1) = Ax_i(k) + B_u u_i(k) + B_w w_i(k) \tag{1}$$

$$x_i(k) = \begin{bmatrix} x_i^{(1)}(k) \\ \dot{x}_i^{(1)}(k) \\ x_i^{(2)}(k) \\ \dot{x}_i^{(2)}(k) \end{bmatrix}, \qquad u_i(k) = \begin{bmatrix} u_i^{(1)}(k) \\ u_i^{(2)}(k) \end{bmatrix}$$
$$w_i(k) = \begin{bmatrix} w_i^{(1)}(k) \\ w_i^{(2)}(k) \end{bmatrix} \tag{2}$$

$$A = \begin{bmatrix} 1 & \Delta T & 0 & 0 \\ 0 & 1 & 0 & 0 \\ 0 & 0 & 1 & \Delta T \\ 0 & 0 & 0 & 1 \end{bmatrix}, \quad B_u = B_w = \frac{1}{m}\begin{bmatrix} \Delta T^2/2 & 0 \\ \Delta T & 0 \\ 0 & \Delta T^2/2 \\ 0 & \Delta T \end{bmatrix} \tag{3}$$

where x_i is the state of spacecraft i in an inertial frame, u_i is the control input, w_i is zero mean white process noise with covariance Q, m is the mass of each spacecraft (assumed to be identical for each spacecraft in the fleet), and ΔT is the sampling time. Two-dimensional systems are presented here for simplicity but the approach is fully generalized to three dimensions. Without loss of generality, the process noises w_i and w_j are considered to be uncorrelated, that is, $E[w_i(k)w_j(k)^T] = 0$.

Given the linear dynamics and the lack of an inertial position sensor, the ith spacecraft maintains estimates of $N-1$ relative states. The relative dynamics are found by subtracting Eq. (1) from itself and replacing i with j,

$$x_{ji}(k+1) = Ax_{ji}(k) + B_u u_{ji}(k) + B_w w_{ji}(k) \tag{4}$$

$$\{x, u, w\}_{ji}(k) \triangleq \{x, u, w\}_j(k) - \{x, u, w\}_i(k) \quad \forall\ j \neq i \tag{5}$$

Note that this requires the mass of each spacecraft to be identical. This is for simplicity; the following treatment can be easily modified when this is not the case. The key is that the state transition matrices are identical across the fleet eliminating the need for inertial states, and thus, inertial state measurements.

Equations (4) and (5) can be rewritten to yield a full set of dynamics *relative* to spacecraft i:

$$\mathbf{x}_i(k+1) = \mathbf{A}\mathbf{x}_i(k) + \mathbf{B_u}\mathbf{u}_i(k) + \mathbf{B_w}\mathbf{w}_i(k) \tag{6}$$

$$\{\mathbf{x},\mathbf{u},\mathbf{w}\}_i(k) \triangleq \left[\begin{array}{c}\vdots\\ \{x,u,w\}_{ji}(k)\\ \vdots\end{array}\right]_{j\in\{1,\ldots,N\}\setminus i} \tag{7}$$

$$\{\mathbf{A},\mathbf{B_u},\mathbf{B_w}\} \triangleq \left[\begin{array}{ccc}\{A,B_u,B_w\} & & \\ & \ddots & \\ & & \{A,B_u,B_w\}\end{array}\right] \tag{8}$$

Equation (7) is read as an augmented vector consisting of the $N-1$ relative vectors defined in Eq. (5) such that $\mathbf{x}_i \in \mathbb{R}^{4(N-1)}$ and $\{\mathbf{u}_i,\mathbf{w}_i\} \in \mathbb{R}^{2(N-1)}$. Similarly, Eq. (8) is block diagonal such that $\mathbf{A} \in \mathbb{R}^{4(N-1)\times 4(N-1)}$ and $\{\mathbf{B_u},\mathbf{B_w}\} \in \mathbb{R}^{4(N-1)\times 2(N-1)}$. It follows from the assumptions that $\mathbf{w}_i$ is zero mean and its covariance is $E[\mathbf{w}_i(j)\mathbf{w}_i(k)^T] = \mathbf{Q}\delta_{jk}$ where

$$\mathbf{Q} = \left[\begin{array}{cccc}2Q & Q & \cdots & Q\\ Q & 2Q & & \vdots\\ \vdots & & \ddots & Q\\ Q & \cdots & Q & 2Q\end{array}\right] \tag{9}$$

The relative state vectors are shown conceptually in Fig. 1.

B. Virtual Center

For formation control, a reference state for each vehicle in the formation must be defined. Following [7], a *virtual center state*, x_c, is defined relative to the desired formation geometry in the inertial reference frame; a local frame centered at x_c is then defined such that the difference between the inertial frame and the virtual center frame is only a translation. A local reference frame at each spacecraft i is similarly defined and the location of the virtual center in the ith local frame is denoted by $x_{ci} = x_c - x_i$, similar in notation to Eq. (5). Over relatively short time horizons, the formation is allowed to drift in the inertial frame. Therefore, it is sufficient to specify the reference states in the virtual center frame, denoted by $r_{ic} \in \mathbb{R}^4 \ \forall\ i \in \{1,\ldots,N\}$. The set of N reference states are arranged in a single column vector as follows:

$$\mathbf{r}\,(k) \triangleq \left[\begin{array}{c}r_{1c}(k)\\ \vdots\\ r_{Nc}(k)\end{array}\right] \in \mathbb{R}^{4N} \tag{10}$$

It is convenient to rearrange this vector for each spacecraft such that, for spacecraft i, its reference state appears first followed by the $N-1$ reference states of the remote spacecraft. Therefore,

$$\mathbf{r}_i(k) \triangleq \left[\begin{array}{c}r_{ic}(k)\\ \mathbf{r}_{ri}(k)\end{array}\right], \in \mathbb{R}^{4N} \qquad \mathbf{r}_{ri}(k) \triangleq \left[\begin{array}{c}\vdots\\ r_{jc}(k)\\ \vdots\end{array}\right]_{j\in\{1,\ldots,N\}\setminus i} \in \mathbb{R}^{4(N-1)} \tag{11}$$

These reference states are assumed to be known to each spacecraft in the system. The relative state, reference state, and error state vectors in the given system are shown in Fig. 1 for a small formation.

C. RBS Measurements

The measurements provided by the RBS are relative range and bearing to a remote spacecraft, each corrupted with white Gaussian noise. Thus, at each time step k, a measurement is made to one or more remote spacecraft,

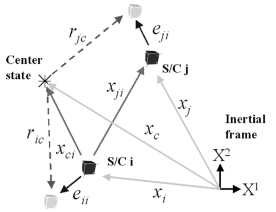

Fig. 1 Virtual center state x_{ci} relative to spacecraft i, denoted by *. Also shown are reference states $r_{\cdot c}$, error states $e_{\cdot i}$, and relative state x_{ji}.

$$\mathbf{z}_i(k) \triangleq \left[\begin{array}{c}\vdots\\ z_{ji}(k)\\ \vdots\end{array}\right]_{j\in M_i(k)} = \mathbf{h}[\mathbf{x}_i(k),k] + \mathbf{v}_i(k) \tag{12}$$

$$z_{ji}(k) = h[x_{ji}(k)] + v_{ji}(k) \tag{13}$$

$$h[x_{ji}(k)] = \left[\begin{array}{c}R_{ji}(k)\\ \phi_{ji}(k)\end{array}\right] = \left[\begin{array}{c}\sqrt{[x_{ji}^{(1)}(k)]^2 + [x_{ji}^{(2)}(k)]^2}\\ \tan^{-1}\frac{x_{ji}^{(2)}(k)}{x_{ji}^{(1)}(k)}\end{array}\right] \tag{14}$$

where v_{ji} is zero mean, white Gaussian noise with covariance R and $M_i(k) \subseteq \{1,\ldots,N\} \setminus i$ is the index set of measurements which may vary with time as selected by switching logic external to the sensor. Note that typically M_i contains only one element when each spacecraft is equipped with a single RBS. Because the spacecraft is also equipped with an inertial attitude sensor, the relative range/bearing measurements are assumed to be made in the inertial frame without loss of generality; the statistical errors present in the attitude sensor are assumed to be built into the RBS noise covariance R. The sensor is assumed to be able to provide measurements at all ranges.

D. Extended Information Filter

At each spacecraft i, estimates of the relative states $\mathbf{x}_i$, denoted by $\hat{\mathbf{x}}_i$, are maintained via an extended information filter (EIF) [16]. The EIF is a convenient choice because it can be used to fuse measurements from multiple sensors, and because the information matrix is used as a weight in the virtual center calculation described in Sec. III. The filter is statistically equivalent to the extended Kalman filter and maintains an information state, $\hat{\mathbf{y}}_i(k \mid l) \triangleq \mathbf{Y}_i(k \mid l)\hat{\mathbf{x}}_i(k \mid l)$, and an information matrix,

$$\mathbf{Y}_i(k \mid l) \triangleq (E\{[\mathbf{x}_i(k) - \hat{\mathbf{x}}_i(k \mid l)][\mathbf{x}_i(k) - \hat{\mathbf{x}}_i(k \mid l)]^T \mid Z^l\})^{-1} \tag{15}$$

where $\hat{\mathbf{x}}_i(k \mid l)$ is the estimate of $\mathbf{x}_i(k)$ given the measurements up to and including time step l, denoted by Z^l. The EIF prediction and update steps are

$$\hat{\mathbf{y}}_i(k \mid k-1) = \mathbf{Y}_i(k \mid k-1)[\mathbf{A}\hat{\mathbf{x}}_i(k-1 \mid k-1) + \mathbf{B_u}\mathbf{u}_i(k)] \tag{16}$$

$$\mathbf{Y}_i(k \mid k-1) = [\mathbf{A}\mathbf{Y}_i^{-1}(k \mid k)\mathbf{A}^T + \mathbf{Q}]^{-1} \tag{17}$$

$$\begin{aligned}\mathbf{y}_i(k \mid k) = \mathbf{y}_i(k \mid k-1) + \mathbf{C}_i(k)^T\mathbf{R}^{-1}(k)\{\mathbf{z}_i(k)\\ - \mathbf{h}[\hat{\mathbf{x}}_i(k \mid k-1),k] + \mathbf{C}_i(k)\hat{\mathbf{x}}_i(k \mid k-1)\}\end{aligned} \tag{18}$$

$$\mathbf{Y}_i(k \mid k) = \mathbf{Y}_i(k \mid k-1) + \mathbf{C}_i(k)^T\mathbf{R}^{-1}(k)\mathbf{C}_i(k) \tag{19}$$

where

$$\mathbf{C}_i(k) = \left[\begin{array}{c}\vdots\\ C_{ji}(k)\\ \vdots\end{array}\right]_{j\in M_i(k)} = \left.\frac{\partial \mathbf{h}}{\partial \mathbf{x}_i}\right|_{\hat{\mathbf{x}}_i(k|k-1)} \tag{20}$$

A useful approximation to the time varying $C_{ji}(k)$ consists of evaluating the Jacobian at the formation reference states. That is,

$$\bar{C}_{ji} = \left.\frac{\partial h}{\partial x_{ji}}\right|_{r_{jc}-r_{ic}} \tag{21}$$

Throughout the paper, an information matrix with a single argument, for example, $\mathbf{Y}(k)$ will be used as shorthand for the updated information matrix, $\mathbf{Y}(k \mid k)$.

E. Time Optimal Controller

An optimal controller (minimum time) based on thrust limited $(u_i^{\{1,2\}}) \in \{-U_{\max}, 0, U_{\max}\}$ propulsion is used in the same vein as that developed in [9]. Because the satellite can be represented with second order free-space dynamics in each axis (decoupled), a feedforward, formation keeping controller based on minimum time optimal control is developed. The controller is activated if the satellite drifts away from its reference position by more than an error ellipse, which is written as

$$[e_{ii}(k)]^T[\mathrm{diag}\{e_{\max}^{(1)}, \dot{e}_{\max}^{(1)}, e_{\max}^{(2)}, \dot{e}_{\max}^{(2)}\}][e_{ii}(k)] > 1 \tag{22}$$

where $e_{\max}^{(\cdot)}$, $\dot{e}_{\max}^{(\cdot)}$ are tuning parameters and $e_{ii}(k) = x_{ci}(k) + r_{ic}(k)$. If this occurs, a minimum time controller is calculated in each axis. For second order dynamics, the minimum time controller is a bang-bang controller with a single switch. Thus, the control is given by

$$u^{(\cdot)}(k) = \begin{cases} -\mathrm{sgn}(e^{(\cdot)} + \dot{e}^{(i)}|\dot{e}^{(\cdot)}|/2)U_{\max}, & 0 < k - k_0 < T_{mt1,i}^{(\cdot)}/T \\ \mathrm{sgn}(e^{(\cdot)} + \dot{e}^{(\cdot)}|\dot{e}^{(\cdot)}|/2)U_{\max}, & T_{mt1,i}^{(\cdot)}/T < k - k_0 < T_{mtF,i}^{(\cdot)}/T \end{cases} \tag{23}$$

where k_0 is the time at the start of the maneuver. The switch time and final control time are written as

$$T_{mt1,i}^{(\cdot)} = \frac{-\dot{e}_{ii}^{(\cdot)}(k) \pm \sqrt{[\dot{e}_{ii}^{(\cdot)}(k)]^2/2 - e_{ii}^{(\cdot)}(k)\bar{U}_{\max}}}{\bar{U}_{\max}} \tag{24}$$

$$T_{mtF,i}^{(\cdot)} = \frac{-\dot{e}_{ii}^{(\cdot)}(k) \pm \sqrt{2[\dot{e}_{ii}^{(\cdot)}(k)]^2 - 4e_{ii}^{(\cdot)}(k)\bar{U}_{\max}}}{\bar{U}_{\max}} \tag{25}$$

where $\bar{U}_{\max} = U_{\max}/m$. It is noted that other control methodologies, such as bounds on relative velocity, minimum fuel, etc., could be used, but this controller is sufficient to evaluate the proposed architecture.

III. Distributed Information Weighted Virtual Center

In [7], it is proposed that the virtual center state is calculated at each time step by minimizing a weighted squared error in the relative formation states under the assumption that minimizing the error minimizes the control effort required to null the error. Relative to spacecraft i, the virtual center is written as

$$x_{ci}^* = \arg\min_{x_{ci}} \mathbf{e}_i^T W_i \mathbf{e}_i \tag{26}$$

$$\mathbf{e}_i = \left[\begin{array}{c} e_{ii} \\ \left[\begin{array}{c}\vdots\\ e_{ji}\\ \vdots\end{array}\right]_{j\in\{1,\ldots,N\}\setminus i}\end{array}\right] \in \mathbb{R}^{4N} \tag{27}$$

$$e_{ii} = x_{ci} + r_{ic} \in \mathbb{R}^4 \tag{28}$$

$$e_{ji} = x_{ci} - (x_{ji} - r_{jc}) \in \mathbb{R}^4 \tag{29}$$

where W_i is an arbitrary symmetric weighting matrix. The errors e_{ji} are referred to as the remote error states and e_{ii} the local error state. In [7], the center state is maintained at a single spacecraft, for example, spacecraft $i = 1$, and W_1 is related to the fuel reserve states of each spacecraft in the fleet. The error state of a spacecraft that has low fuel is given a higher weight than that of a spacecraft with higher fuel, reducing the error and thus the control effort of the low fuel spacecraft. This has the advantage of balancing fuel across the fleet; however, this approach is centralized and communication intensive because spacecraft 1 must transmit the resulting center state to the fleet at each time step. Another disadvantage is that it relies on $N-1$ accurate relative state estimates $\hat{\mathbf{x}}_1$ at spacecraft 1. Estimates of each relative state can be maintained at spacecraft 2 through N and transmitted to spacecraft 1 to reduce the computational load, however, this would require additional communication bandwidth.

A. Distributed Virtual Center

A decentralized implementation of the virtual center algorithm is proposed here where each spacecraft in the fleet calculates a local estimate of the virtual center $\hat{x}_{ci} = E[x_{ci}]\ \forall\ i \in \{1,\ldots,N\}$ based on relative state estimates using measurements generated by local sensors. If each spacecraft maintains $N-1$ noise-free relative states and uses identical weights ($W_i = I$), then the resulting center states are equivalent, that is, $\hat{x}_{ci} + x_i = \hat{x}_{cj} + x_j\ \forall\ i, j \in \{1,\ldots,N\}$, equivalent to the centralized implementation in [7]. This implementation, although decentralized, is infeasible as it requires $N-1$ noise-free range/bearing sensors.

Rewriting the center state in Eq. (26) at spacecraft i in terms of the $N-1$ relative state estimates, $\hat{\mathbf{x}}_i$, yields

$$\hat{x}_{ci} = \arg\min_{x_{ci}}[\Phi x_{ci} - (\Gamma\hat{\mathbf{x}}_i - \mathbf{r}_i)]^T W_i[\Phi x_{ci} - (\Gamma\hat{\mathbf{x}}_i - \mathbf{r}_i)]$$
$$\Phi = \left[\begin{array}{c} I_4 \\ \vdots \\ I_4 \end{array}\right], \qquad \Gamma = \left[\begin{array}{c} 0_{4\times 4(N-1)} \\ I_{4(N-1)} \end{array}\right] \tag{30}$$

The well-known solution to this linear least squares problem is

$$\hat{x}_{ci} = (\Phi^T W_i \Phi)^{-1}\Phi^T W_i(\Gamma\hat{\mathbf{x}}_i - \mathbf{r}_i) \tag{31}$$

$$= \left(\sum_{j=1}^{N}\sum_{k=1}^{N}[W_i]_{jk}\right)^{-1}\Phi^T W_i(\Gamma\hat{\mathbf{x}}_i - \mathbf{r}_i) \tag{32}$$

where $[\cdot]_{jk}$ denotes the jkth 4-by-4 subblock of $\cdot$. The covariance of the center state is

$$\mathbf{P}_{ci} = E[(x_{ci} - \hat{x}_{ci})(x_{ci} - \hat{x}_{ci})^T] \tag{33}$$

$$= (\Phi^T W_i \Phi)^{-1}\Phi^T W_i \Gamma \mathbf{P}_i \Gamma^T W_i \Phi (\Phi^T W_i \Phi)^{-1} \tag{34}$$

$$= \left(\sum_{j=1}^{N}\sum_{k=1}^{N}[W_i]_{jk}\right)^{-1}\left(\sum_{j=1}^{N}\sum_{k=1}^{N}[W_i\Gamma\mathbf{P}_i\Gamma^T W_i]_{jk}\right)\left(\sum_{j=1}^{N}\sum_{k=1}^{N}[W_i]_{jk}\right)^{-1} \tag{35}$$

where $\mathbf{P}_i = \mathbf{Y}_i^{-1}$ is the covariance of the relative state estimates. Care must be taken when choosing the weights W_i because the covariance of the center state estimate can become large or infinite if the covariance of any of the relative states of the spacecraft are large or infinite, corresponding to poorly observed or unobserved remote

spacecraft, which is an inherent trait of the system given the large number of spacecraft.

B. Information Weighted Virtual Center

The distributed algorithm in Sec. III.A can run locally at the spacecraft with any number of $n \leq N-1$ relative state estimates to solve for the virtual center. Thus, if any spacecraft are poorly observed, the corresponding entries in W_i can be set to zero to avoid numerical problems and to accurately calculate the virtual center. In the limiting case, where $n=0$ at spacecraft i, the virtual center estimate reduces to $\hat{x}_{ci} = -r_{ic}$. In this case, the spacecraft does not perform any correcting maneuvers because the error state is $e_{ii} = \hat{x}_{ci} + r_{ic} = 0$. This idea can be generalized by incorporating the information content of the relative state estimates $\hat{\mathbf{x}}_i$, contained in $\mathbf{Y}_i$, in the weighting matrix W_i. In other words, states with high information (low uncertainty) are weighted more in the calculation. Because $\mathbf{Y}_i$ serves as a weight on only the remote error states $e_{ji}\ \forall\ j \in [1,N] \setminus i$, a weight on the local error state e_{ii}, denoted by G_i is introduced such that

$$W_i = \begin{bmatrix} G_i & \\ & \mathbf{Y}_i \end{bmatrix} \tag{36}$$

This form of the weighting matrix has the benefit of preventing any poorly observed spacecraft from hindering the virtual center estimate. Substituting the above into Eqs. (32) and (35), and inverting Eq. (35) to yield the center state information matrix yields

$$\hat{x}_{ci} = \left(G_i + \sum_{j=1}^{N-1}\sum_{k=1}^{N-1} [\mathbf{Y}_i]_{jk} \right)^{-1} [\Phi^T \mathbf{Y}_i (\hat{\mathbf{x}}_i - \mathbf{r}_{ri}) - G_i r_{ic}] \tag{37}$$

$$\mathbf{Y}_{ci} = \mathbf{P}_{ci}^{-1} = \left(G_i + \sum_{j=1}^{N-1}\sum_{k=1}^{N-1} [\mathbf{Y}_i]_{jk} \right) \left(\sum_{j=1}^{N-1}\sum_{k=1}^{N-1} [\mathbf{Y}_i]_{jk} \right)^{-1} \left(G_i + \sum_{j=1}^{N-1}\sum_{k=1}^{N-1} [\mathbf{Y}_i]_{jk} \right) \tag{38}$$

In this formulation, unobserved (poorly observed) spacecraft correspond to zero (near zero) information on the unobserved states, resulting in a zero (near zero) weight on those states in the virtual center calculation. In such a case, the order of the filter, and the order of the associated center state calculation, may be reduced to eliminate the states corresponding to the unobserved or poorly observed spacecraft. Such reductions, however, can lead to an unstable formation. For instance, in a two spacecraft system, spacecraft 1 need not maintain a good estimate of the state of spacecraft 2 as long as spacecraft 2 is monitoring spacecraft 1; this is the typical leader–follower scheme. However, if spacecraft 2 has a poor estimate of spacecraft 2, the spacecraft will drift apart. More detailed discussion of the connectivity requirements is given in the next section.

C. Interpretation of Information Weighting: Control Dependency Graph

Using the information matrix as a weight also has a direct effect on the control dependency graph (CDG). The CDG is a directed graph that illustrates the dependency of each local controller on the state of each spacecraft in the formation [6]. Typically, the dependencies are considered binary with respect to the local control laws: either there is or there is not a dependency. However, the virtual center calculation allows for a continuum of dependency that is based on the entries in the weighting matrices W_i. Considering spacecraft i, if the weight on the relative state of a particular spacecraft j tends to zero, then state x_{ji} does not factor into the calculation. If the same weight goes to infinity, then the virtual center approaches $x_{ji} - r_{jc}$ reducing spacecraft i to a simple follower of spacecraft j.

Consider the CDGs in Fig. 2, where an arrow from spacecraft i to j denotes a dependency of the control on spacecraft j on the state of spacecraft i. The formation in the upper left results from $\mathbf{Y}_{ij} \neq 0$ and $G_i < \infty\ \forall\ i,j$. Spacecraft 1 is made a leader when $\mathbf{Y}_1 = 0$ (equivalently, $G_1 \to \infty$), resulting in the CDG in the upper right. Spacecraft 3 becomes a follower of spacecraft 4 when $\mathbf{Y}_{31} = \mathbf{Y}_{32} = 0$, $\mathbf{Y}_{34} \neq 0$, resulting in the CDG in the lower left. The formation in the lower right is unstable as both spacecraft 1 and 3 are leaders. In this case, the system as a whole is unstable, and therefore spacecraft 1 and 3 will begin to drift and the formation will stretch or contract depending on the relative motion of spacecraft 1 and 3. Spacecraft 2 and 4 will attempt, unsuccessfully, to maintain their desired relative states to both spacecraft 1 and 3. Such a fault is detectable at spacecraft 2 and 4 by evaluating the center state cost in Eq. (26). As the formation stretches or contracts, the center state cost will grow; if it reaches some threshold, a fault can be considered to have occurred and appropriate measures may be taken. These measures would consist of finding the source of the fault, of which the possibilities are numerous. The fault may be due to an error in the controller, or a bad actuator. It may also be due to errors in the inertial attitude determination subsystem. In cases such as these, if the fault cannot be corrected, the spacecraft should be removed from the formation and parked at a safe distance. If this is not possible, it may be necessary to move the formation to a safe distance while the problem is being addressed. If the problem lies within the sensing and estimation subsystem as described above, however, an algorithm can be developed that would traverse the CDG to find broken or weak links due to low information. If such links are found, the faulty spacecraft can attempt to reestablish the broken link by reinitializing the sensor/estimator, possibly with estimates that are communicated to it from other spacecraft, or the spacecraft can be isolated from the formation while diagnostics can be performed.

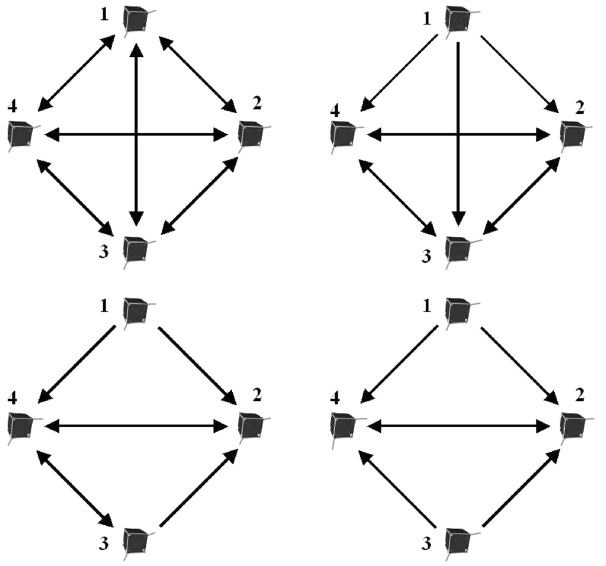

Fig. 2 Control dependency graphs (CDG) for a four spacecraft system. The formation in the lower right is unstable as it consists of two independent leaders: spacecraft 1 and 3.

These observations lead to a necessary, but not sufficient, condition for formation stability: that there exists at least one spacecraft from which there extends a path along the CDG to every other spacecraft in the formation. Stability in this case is defined as the formation being able to drive the relative error to zero in the local reference frame.

D. Hybrid Leader Follower Using G_i

The free weights G_i in Eq. (36) can also be used to control the degree to which each spacecraft "leads" or "follows" the fleet, thus allowing the designer to select a hybrid mix of leader follower for each spacecraft. For example, in a two spacecraft system, and $G_1 = \infty$ and $G_2 = 0$, a leader–follower scheme results where spacecraft 1 is the leader (drifts with no control) and 2 is the follower. It is proposed to define G_i in the general problem for N spacecraft as the

following:

$$G_i = \frac{g_i}{N-1}\sum_{j=1}^{N-1}\sum_{k=1}^{N-1}[\mathbf{Y}_i]_{jk} + c \cdot I \tag{39}$$

This term is an average of the weights on the $N-1$ remote error states (or equivalently, an average of the information of the remote relative states) weighted by g_i, and an additive weight $c \cdot I$. The constant $c \cdot I$ is necessary to keep the inverse in Eq. (37) from becoming singular; as such, c can be made relatively small. Substituting Eq. (39) into Eqs. (37) and (38), the resulting center state estimate and information matrix at spacecraft i are

$$\hat{x}_{ci} = \left[c \cdot I + \left(1 + \frac{g_i}{N-1}\right)\sum_{j=1}^{N-1}\sum_{k=1}^{N-1}[\mathbf{Y}_i]_{jk}\right]^{-1}\left[\Phi^T\mathbf{Y}_i(\hat{\mathbf{x}}_i - \mathbf{r}_{ri}) - \left(c \cdot I + \frac{g_i}{N-1}\sum_{j=1}^{N-1}\sum_{k=1}^{N-1}[\mathbf{Y}_i]_{jk}\right)r_{ic}\right] \tag{40}$$

$$\mathbf{Y}_{ci} = \left(1 + \frac{g_i}{N-1}\right)^2\left(\sum_{j=1}^{N-1}\sum_{k=1}^{N-1}[\mathbf{Y}_i]_{jk}\right) + 2c\left(1 + \frac{g_i}{N-1}\right)I + c^2\left(\sum_{j=1}^{N-1}\sum_{k=1}^{N-1}[\mathbf{Y}_i]_{jk}\right)^{-1} \tag{41}$$

Note that as $\mathbf{Y}_i$ approaches zero, perhaps as a result of a failure of the RBS on spacecraft i and a lack of measurements provided to the EIF, $\mathbf{Y}_{ci}$ approaches ∞. Thus the center state estimate $\hat{x}_{ci}$ approaches a constant $-r_{ic}$, as it should, and no control is spent.

The designer can now adjust g_i to fit mission specific needs. In missions such as SI, which consist of a single large hub spacecraft and $N-1$ smaller reflector spacecraft, it may be desirable to place a g_i on the hub spacecraft that is different from the reflector spacecraft, depending on the mission phase. If the formation is in the observation phase, it may be necessary to make the hub spacecraft an effective leader. This may also be the case if the system is designed such that the hub is responsible for stabilizing the orbit of the formation about L_2. The hub is made a leader by setting $q_{\text{hub}} = \infty$ during such orbit corrections. Given the position of the hub in the inertial frame, trajectories in the inertial frame for the follower spacecraft can easily be translated via the reference states $\mathbf{r}(k)$. Conversely, the weight on the hub spacecraft may be lowered during housekeeping activities.

The scalar g_i can also be used to incorporate the local fuel reserve state by allowing g_i to approach ∞ for low fuel, and some small value or zero for high fuel. As an example, the constant g_i could be chosen based on the function $g_i(F_i) = a/F_i + b$ where $F_i \in [0, 1]$ is the normalized fuel reserve state, and a and b are tuning parameters that can be chosen, for example, by choosing g_i values when the spacecraft's fuel reserves are full, and half-full. Denoting these values, respectively, as q_i^{full} and q_i^{half} such that $g_i^{\text{full}} < g_i^{\text{half}}$ yields

$$g_i(F_i) = \frac{g_i^{\text{half}} - g_i^{\text{full}}}{F_i} + 2g_i^{\text{full}} - g_i^{\text{half}} \tag{42}$$

IV. Sensor Scheduling

Spacecraft in formation-based missions such as SI will most likely be equipped with only a single RBS, and therefore, only a single range/bearing measurement is provided at each time step. Thus, an algorithm is introduced which switches the measurements of the RBS among the spacecraft based on maximizing a function of the information matrix. Maximizing both the center state information and formation information is considered. The general sensor scheduling problem, first described in [10] has been addressed in many settings. Many approaches [10–12] attempt to find a schedule over a short time horizon and use heuristic algorithms to solve for optimal and near-optimal sequences. However, because most future spacecraft missions consider long time horizons with respect to the sampling rate, it is proposed here to pose the problem as finding a schedule that minimizes a function of the covariance (or information) in an infinite time horizon. If the optimal measurement schedule can be represented by a simple measurement control law or stored in a lookup table, less computation will be required to determine the measurement at each time step.

A. Infinite Time Sensor Scheduling Problem

Considering a single spacecraft (omitting the i subscripts) and a single measurement, the finite time horizon sensor scheduling problem is cast as minimizing a cost function,

$$J_{K_F} \triangleq \frac{1}{K_F}\text{trace}\sum_{k=1}^{K_F} f[\mathbf{Y}(k)] \tag{43}$$

where $\mathbf{Y}(k)$ is the updated information matrix as a function of sensor selection decision variables. It evolves according to Eqs. (17) and (19) which can be simplified to an information form of the Riccati equation

$$\mathbf{Y}(k+1) = \mathbf{A}^{-T}\mathbf{Y}(k)\mathbf{A}^{-1} + \mathbf{C}(k)^T R(k)^{-1}\mathbf{C}(k) - \mathbf{A}^{-T}\mathbf{Y}(k)\mathbf{A}^{-1}\mathbf{B}_{\mathbf{w}}[\mathbf{B}_{\mathbf{w}}{}^T\mathbf{A}^{-T}\mathbf{Y}(k)\mathbf{A}^{-1}\mathbf{B}_{\mathbf{w}} + \mathbf{Q}^{-1}]^{-1}\mathbf{B}_{\mathbf{w}}{}^T\mathbf{A}^{-T}\mathbf{Y}(k)\mathbf{A}^{-1} \tag{44}$$

The measurement matrices $\mathbf{C}(k)$ are selected from the finite measurement set $\mathbf{C}(k) \in \{\bar{C}_{ji} \mid j \in N_i\}$, with corresponding measurement noise covariances $R(k) \in \{R_{ji} \mid j \in N_i\}$ where N_i is an index set of available measurements, via the measurement control law $\boldsymbol{\mu}_{K_F} = \{\mu(1), \ldots, \mu(K_F)\}$ such that $\mu(k) \in N_i$ and $\mathbf{C}(k) = \bar{C}_{\mu(k)i}$. For the fleet estimation problem outlined in Sec. II, the index set is the set of remote spacecraft measurements $N_i = \{1, \ldots, N\} \setminus i$. Without loss of generality, the sensor noise covariance is assumed to be identical for all measurements and will be denoted by $\mathbf{R}$, that is, $R_{ji} = R_{ki} = \mathbf{R}\ \forall\ j, k \in N_i$. Because what follows is dependent on a fixed number of (approximately) constant measurement matrices, the resulting scheduling algorithm is therefore appropriate only for fixed formations with constant reference states $\mathbf{r}$.

Several cost functions are considered, consisting of, respectively, maximizing the center state information (CI) and formation information (FI), and minimizing the center state covariance (CC) and formation covariance (FC):

$$J_{K_F}^{\text{CI}} \triangleq -\frac{1}{K_F}\text{trace}\sum_{k=1}^{K_F}\Phi^T\mathbf{Y}(k)\Phi \tag{45}$$

$$J_{K_F}^{\text{FI}} \triangleq -\frac{1}{K_F}\text{trace}\sum_{k=1}^{K_F}\mathbf{Y}(k) \tag{46}$$

$$J_{K_F}^{\text{CC}} \triangleq \frac{1}{K_F}\text{trace}\sum_{k=1}^{K_F}[\Phi^T\mathbf{Y}(k)\Phi]^{-1} \tag{47}$$

$$J_{K_F}^{\text{FC}} \triangleq \frac{1}{K_F}\text{trace}\sum_{k=1}^{K_F}\mathbf{Y}(k)^{-1} \tag{48}$$

The summation is important to give an average over the full period K. Note that the information costs $J_{K_F}^{\text{CI}}$ and $J_{K_F}^{\text{FI}}$ are defined in the negative to allow minimization.

The infinite time problem consists of minimizing $J_\infty^{(\cdot)} = \lim_{K_F\to\infty} J_{K_F}^{(\cdot)}$ with corresponding measurements $\boldsymbol{\mu}_\infty$. An analytical solution to this general problem has not yet been found. In a recent paper by Gupta and Murray [12], the sensor schedule is

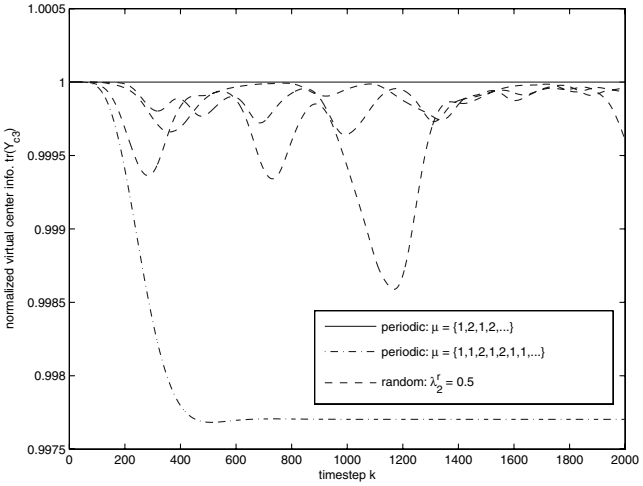

Fig. 3 Comparison of periodic and random measurement sequences.

modeled as a random process such that at each time step, a measurement j is selected from the measurement set N_i with probability λ_j^r, with the constraint

$$\sum_{j\in N_i}\lambda_j^r = 1 \tag{49}$$

The algorithm in [12] solves for the set of probabilities that minimize an upper bound on the expected value of the covariance, which is determined by a set of Riccati-like equations. Although the algorithm produces the optimal λ_j^r, it converges only for stable systems and can be shown to be suboptimal for the formation keeping problem. Consider the scheduling of a single RBS for a three spacecraft system, where spacecraft 1 and 2 are equidistant to spacecraft 3, which is estimating the virtual center based on measurements and estimates to spacecraft 1 and 2. Figure 3 shows the center state information for several random and periodic sequences. The figure shows that the instantaneous information of the random sequence is always less than that of the periodic sequence with measurement sequence $\boldsymbol{\mu} = \{1, 2, 1, 2, \ldots\}$.

B. Periodic Sensor Scheduling Problem

It is proposed that the optimal infinite horizon measurement sequence for any linear time-invariant system is periodic. This was originally suggested in [13], and an algorithm to find the optimal periodic measurements based on generating sequences at random was developed. Here, the periodic formulation is posed as finding the periodic measurement sequence that minimizes $J_\infty^{(\cdot)}$. Thus for a given periodic measurement sequence,

$$\boldsymbol{\mu}_\infty = \{\bar{\boldsymbol{\mu}}_K, \bar{\boldsymbol{\mu}}_K, \ldots\}, \qquad \bar{\boldsymbol{\mu}}_K = \{\bar{\mu}(0), \bar{\mu}(1), \ldots, \bar{\mu}(K-1)\} \tag{50}$$

where K is the (dimensionless) period of the sequence, and the resulting cost is

$$J_\infty^{(\cdot)} = \frac{1}{K}\operatorname{trace}\sum_{k=0}^{K-1} f[\mathbf{Y}^p(k_0+k)] \tag{51}$$

where $\mathbf{Y}^p(k)$ is a steady-state periodic information matrix which is found by solving a periodic Riccati equation [17], k_0 is an arbitrary constant and f corresponds to the variants in Eqs. (45–48).

The information resulting from a periodic measurement sequence can be determined by a modified algebraic Riccati equation. Using the periodic identity $C(k) = C(\tau K + k)\ \forall\ \tau, k \in \{0, 1, \ldots\}$, the periodic system is represented by the time-invariant dynamics,

$$\tilde{\mathbf{x}}(\tau+1) = \tilde{\mathbf{A}}\,\tilde{\mathbf{x}}(\tau) + \tilde{\mathbf{B}}_{\mathbf{w}}\tilde{\mathbf{w}}(\tau) \tag{52}$$

$$\tilde{\mathbf{z}}(\tau) = \tilde{\mathbf{C}}_{\tau K}\tilde{\mathbf{x}}(\tau) + \tilde{\mathbf{D}}_{\tau K}\tilde{\mathbf{w}}(\tau-1) + \tilde{\mathbf{v}}(\tau) \tag{53}$$

$$\tilde{\mathbf{x}}(\tau) \triangleq \mathbf{x}(\tau K) \tag{54}$$

$$\tilde{\mathbf{w}}(\tau) \triangleq [\mathbf{w}(\tau K)^T \cdots \mathbf{w}(\tau K + K - 1)^T]^T \tag{55}$$

$$\tilde{\mathbf{z}}(\tau) \triangleq [\mathbf{z}(\tau K - K + 1)^T \cdots \mathbf{z}(\tau K)^T]^T \tag{56}$$

$$\tilde{\mathbf{v}}(\tau) \triangleq [\mathbf{v}(\tau K - K + 1)^T \cdots \mathbf{v}(\tau K)^T]^T \tag{57}$$

$$\tilde{\mathbf{A}} \triangleq \mathbf{A}^K \tag{58}$$

$$\tilde{\mathbf{B}}_{\mathbf{w}} \triangleq [\mathbf{A}^{K-1}\mathbf{B}_{\mathbf{w}}\ \mathbf{A}^{K-2}\mathbf{B}_{\mathbf{w}} \cdots \mathbf{B}_{\mathbf{w}}] \tag{59}$$

$$\tilde{\mathbf{C}}_k \triangleq \begin{bmatrix} \mathbf{C}(k-K+1)\mathbf{A}^{-(K+1)} \\ \mathbf{C}(k-K+2)\mathbf{A}^{-(K+2)} \\ \vdots \\ \mathbf{C}(k) \end{bmatrix} \tag{60}$$

$$[\tilde{\mathbf{D}}_k]_{ij} \triangleq \begin{cases} -\mathbf{C}(k-K+i)\mathbf{A}^{i-j}\mathbf{B}_{\mathbf{w}} & \text{if } i < j \\ 0 & \text{otherwise} \end{cases} \tag{61}$$

The matrices in Eqs. (52) and (53) are time invariant with respect to τ when the system dynamics are time invariant and the measurements are periodic with period K. Thus an EIF can be run on the system represented by Eqs. (52) and (53) and will yield an identical estimate and information matrix as when running the EIF on the system represented by Eqs. (6) and (12). The information matrix prediction step is

$$\tilde{\mathbf{Y}}(\tau+1 \mid \tau) = [\tilde{\mathbf{A}}\,\tilde{\mathbf{Y}}(\tau \mid \tau)^{-1}\tilde{\mathbf{A}}^T + \tilde{\mathbf{B}}_{\mathbf{w}}\tilde{\mathbf{Q}}\tilde{\mathbf{B}}_{\mathbf{w}}^T]^{-1} \tag{62}$$

where $\tilde{\mathbf{Q}} \triangleq \operatorname{diag}(\mathbf{Q}, \ldots, \mathbf{Q})$. This equation is the standard EIF prediction equation analogous to Eq. (17). However, the $\tilde{\mathbf{D}}_{\tau K}\tilde{\mathbf{w}}(\tau - 1)$ term in Eq. (53) leads to a nonstandard update step

$$\begin{aligned}\tilde{\mathbf{Y}}(\tau+1 \mid \tau+1) = \tilde{\mathbf{Y}}(\tau+1 \mid \tau) + [\tilde{\mathbf{C}}_{\tau K}^T + \tilde{\mathbf{Y}}(\tau+1 \mid k)\tilde{\mathbf{S}}_{\tau K}]\cdot[\tilde{\mathbf{R}} \\ + \tilde{\mathbf{D}}_{\tau K}\tilde{\mathbf{Q}}\tilde{\mathbf{D}}_{\tau K}^T + \tilde{\mathbf{S}}_{\tau K}^T\tilde{\mathbf{Y}}(\tau+1 \mid \tau)\tilde{\mathbf{S}}_{\tau K}]^{-1}[\tilde{\mathbf{C}}_{\tau K}^T \\ + \tilde{\mathbf{Y}}(\tau+1 \mid \tau)\tilde{\mathbf{S}}_{\tau K}]^T\end{aligned} \tag{63}$$

where $\tilde{\mathbf{S}}_{\tau K} \triangleq \tilde{\mathbf{B}}_{\mathbf{w}}\tilde{\mathbf{Q}}\tilde{\mathbf{D}}_{\tau K}^T$ and $\tilde{\mathbf{R}} \triangleq \operatorname{diag}(\mathbf{R}, \ldots, \mathbf{R})$. The information matrix $\tilde{\mathbf{Y}}(\tau \mid \tau)$ is the information matrix corresponding to the state estimate $\mathbf{x}(\tau K)$, that is, $\tilde{\mathbf{Y}}(\tau \mid \tau) = \mathbf{Y}(\tau K)$.

V. Numerical Solution

The cost associated with a given sequence $\bar{\boldsymbol{\mu}}_K$ can be determined by combining Eqs. (62) and (63) and setting $\tilde{\mathbf{Y}}(\tau+1 \mid \tau+1) = \tilde{\mathbf{Y}}(\tau \mid \tau) = \mathbf{Y}^p(\tau K)$, solving for $\mathbf{Y}^p(\tau K)$ and propagating the result forward $K-1$ times via Eq. (44) to solve for $\mathbf{Y}^p(\tau K + i)$, $i \in \{1, \ldots, K-1\}$. Finding the optimal $\bar{\boldsymbol{\mu}}_K$ using an exhaustive search would require repeating this process $|N_i|^K$ times, where typically $|N_i| = N - 1$ if all spacecraft are observed. This could be computationally expensive for large N or K.

A relaxation of the scheduling problem can be shown to be convex in a set of variables which correspond to the number of measurements made to each spacecraft, normalized by the period K. These variables are denoted by λ_j where $\lambda_j = |\{k \mid \bar{\boldsymbol{\mu}}_K(k) = j\}|/K \ \forall \ j \in N_i$ and each λ_j represents a quantity similar to the λ_j^r defined in [12] where each λ_j can be interpreted as a duty cycle value. For example, if measurements are being made to two spacecraft, denoted by 1 and 2, and if $\lambda_1 = 0.1$ and $\lambda_2 = 0.9$, then 10% of the duty is spent measuring range and bearing to spacecraft 1 and 90% is spent on spacecraft 2. The set of λ_j shall be denoted by Λ such that $\Lambda \triangleq \{\lambda_j \mid j \in N_i\}$. Clearly, $\sum_{j\in N_i}\lambda_j = 1$ and $\lambda_j K$ is constrained to be an integer such that $\lambda_j \in \{0, 1/K, 2/K, \ldots, 1\}$. If the integer constraint is relaxed such that $\lambda_j \in [0, 1]$, then the optimal set of duty cycles can be found by solving a linear matrix inequality (LMI) problem. Note that there are many sequences $\bar{\boldsymbol{\mu}}_K$ which satisfy a given Λ.

Based on the convexity of the relaxed version of the scheduling problem, a two-level algorithm is developed to solve for the optimal measurement schedule for a given K: 1) a (nonexhaustive) steepest descent search over the set of all possible Λ, and 2) for each Λ a (nonexhaustive) search over all possible $\bar{\boldsymbol{\mu}}_K$. The remainder of this section consists of a description of this algorithm and the results of the algorithm as applied to a simple system consisting of three spacecraft. Denoted by 1, 2, and 3, spacecraft 3 is equipped with a single RBS. The spacecraft are nominally located at the vertices of an equilateral triangle in the x–y plane such that spacecraft 3 is at the origin, spacecraft 1 is located 50 m from spacecraft 3 at a bearing of $-\pi/6$ rad from the y axis, and spacecraft 2 is located 50 m from spacecraft 3 at a bearing of $+\pi/6$ rad from the y axis. This example is used to explore the trends and solutions associated with the sensor scheduling problem. It should be noted that the trends described in this section have been observed for larger and more complex systems.

Section V.A outlines the steepest descent search algorithm for the optimal Λ on the relaxed version of the problem, Sec. V.B presents a modification of the steepest descent search algorithm to find the true cost using three different methods of finding a suitable measurement sequence $\bar{\boldsymbol{\mu}}_K$, and Sec. V.C is a modified version of the algorithm that allows for a constraint on the minimum switching time of the RBS.

A. Duty Cycle Search (DCS)

For a fixed Λ, the LMI solution to the relaxed version of the problem can be rewritten as the solution to the Riccati equation

$$\begin{aligned}\hat{\mathbf{Y}} = \tilde{\mathbf{A}}^{-T}\hat{\mathbf{Y}}\tilde{\mathbf{A}}^{-1} - \tilde{\mathbf{A}}^{-T}\hat{\mathbf{Y}}\tilde{\mathbf{A}}^{-1}\tilde{\mathbf{B}}_{\mathbf{w}}(\tilde{\mathbf{B}}_{\mathbf{w}}^{T}\tilde{\mathbf{A}}^{-T}\hat{\mathbf{Y}}\tilde{\mathbf{A}}^{-1}\tilde{\mathbf{B}}_{\mathbf{w}} \\ + K\tilde{\mathbf{Q}}^{-1})^{-1}\tilde{\mathbf{B}}_{\mathbf{w}}^{T}\tilde{\mathbf{A}}^{-T}\hat{\mathbf{Y}}\tilde{\mathbf{A}}^{-1} + K\hat{\mathbf{I}}\end{aligned} \tag{64}$$

where

$$\hat{\mathbf{Y}} = \sum_{i=0}^{K-1}\mathbf{Y}^{p}(\tau K + i) \tag{65}$$

$$\hat{\mathbf{I}} = \sum_{j\in N_i}\lambda_j\bar{\mathbf{I}}_j \tag{66}$$

$$\bar{\mathbf{I}}_j = \sum_{i=0}^{K-1}(\mathbf{A}^{-i})^{T}C_j^{T}R^{-1}C_j\mathbf{A}^{-i} \tag{67}$$

with cost

$$\hat{J}_{\infty}^{(\cdot)} = \frac{1}{K}\mathrm{trace}f(\hat{\mathbf{Y}}) \tag{68}$$

Given the convexity of the relaxed problem in Λ, a steepest descent search algorithm is developed, shown in Algorithm 1. The convexity over the unconstrained Λ guarantees convergence for small step size $\Delta\lambda$, however, the algorithm may converge slowly. For faster convergence, the step size may be set to $1/K$, which has the added benefit of satisfying the integer constraint on Λ.

Algorithm 1 Steepest descent search algorithm for optimal duty cycles

```
1:  procedure GradMinCost(Λ_0)
2:      Λ* ← Λ_0, J* ← ∞, m ← 1
3:      while done = FALSE do
4:          Λ^m ← Λ*, done ← TRUE
5:          for j, k ∈ N_i, j ≠ k do
6:              Λ^{m+1} ← Λ^m
7:              λ_j^{m+1} ← λ_j^{m+1} + Δλ
8:              λ_k^{m+1} ← λ_k^{m+1} − Δλ
9:              J^{m+1} ← Ĵ_∞^{(·)}(Λ^{m+1})
10:             if J^{m+1} < J* then
11:                 Λ* ← Λ^{m+1}, J* ← J^{m+1}, done ← FALSE
12:             end if
13:         end for
14:         m ← m + 1
15:     end while
16: end procedure

17: function J = Ĵ_∞^{(·)}(Λ)
18:     Solve Eq. (64) for Ŷ
19:     J ← trace f(Ŷ)/K
20: end function
```

Figure 4 shows the results of the algorithm for the duty cycles Λ on the three spacecraft system using the information-based cost functions J_{∞}^{CI} and J_{∞}^{FI}. Because of the constraint $\lambda_1 + \lambda_2 = 1$, the cost as a function of only λ_1 is shown. The increase in information with K for the DCS case is due to the lack of the cross-covariance terms in the LMI-based cost. The results suggest that, although K is always necessarily greater than 1, it is sufficient to solve the LMI for $K = 1$ because the solutions for Λ are identical for each K and yield cost that is closest to the truth solution. This is advantageous because the dimension of $\tilde{\mathbf{Q}}$ in Eq. (64) grows with increasing K. The resulting Λ can be rounded up or down to meet the integer constraint and can then be used as an initial guess for the sequence search (SS) algorithm.

B. Sequence Search

The convexity of the relaxed version of the problem as described in the previous section suggests that a steepest descent search algorithm may be used for the full problem as well. The SS algorithm is therefore identical to the DCS algorithm in Algorithm 1 with the exception of the cost function evaluation in line 9. For the SS algorithm, this function consists of choosing a sequence $\bar{\boldsymbol{\mu}}_K$ which satisfies the duty cycles Λ and evaluating the cost $J_{\infty}^{(\cdot)}$ by solving

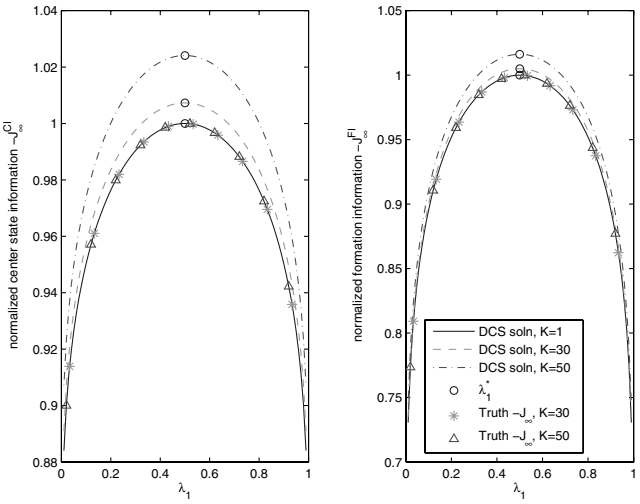

Fig. 4 DCS results for $K = 1, 30, 50$. Shown is the optimal λ_1^* found for each case using DCS, the relaxed cost $\hat{J}_{\infty}^{(\cdot)}$ for all Λ, and the truth cost $J_{\infty}^{(\cdot)}$ found by the solution to the Riccati equation described in Sec. V.B.

Algorithm 2 Sequence search cost function for the steepest descent search algorithm

```
function J = J_∞^(∪)(Λ)
    Generate μ̄_K
    Solve Eqs. (62) and (63) for Y^p(τK)
    Find Y^p(τK + i) for i ∈ {1, ..., K − 1} via Eq. (44)
    J ← [trace Σ_{k=0}^{K−1} f(Y^p(τK + k))]/K
end function
```

Algorithm 3 Sequence search algorithm for fast measurement sequences

```
function μ̄*(μ̄_0)
    μ̄* ← μ̄_0, J* ← ∞, m ← 1
    while done = FALSE do
        μ̄^m ← μ̄*, done ← TRUE
        for j, k ∈ {1, ..., K}, j ≠ k do
            μ̄^{m+1} ← μ̄^m
            μ̄^{m+1}(j) ← μ̄^m(k)
            μ̄^{m+1}(k) ← μ̄^m(j)
            J^{m+1} ← result of Eq. (70)
            if J^{m+1} < J* then
                μ̄* ← μ̄^{m+1}, J* ← J^{m+1}, done ← FALSE
            end if
        end for
        m ← m + 1
    end while
end function
```

Eqs. (62) and (63) for the steady-state periodic information matrix $\mathbf{Y}^p(\tau K)$, propagating the result via Eq. (44) to find $\mathbf{Y}^p(\tau K + i)$ for $i \in \{1, \ldots, K-1\}$ and Eq. (51) to find the cost. Clearly, for the SS algorithm it is necessary to set $\Delta\lambda = 1/K$. This modification is shown in Algorithm 2.

The SS algorithm requires a specific measurement sequence for a given Λ. There are, however, many sequences that yield the same Λ. In the three spacecraft example, let $K = 6$ and consider the measurement sequence on spacecraft 3 such that $\Lambda = \{\lambda_1, \lambda_2\} = \{0.5, 0.5\}$. Three sequences that match these parameters are $\{1, 2, 1, 2, 1, 2\}$, $\{1, 1, 1, 2, 2, 2\}$, and $\{1, 1, 2, 2, 1, 2\}$. There are others, but these three are of interest because they are considered, in some sense, to be the fastest, the slowest, and the intermediate, respectively. To quantify the switching speed, a variance in the sampling times to each spacecraft is defined. For a given sequence $\bar{\boldsymbol{\mu}}_K$, the set of times between each sample to spacecraft j is

$$\Delta k_j = \{n - m : \mu(m) = \mu(n) = j,\ \mu(p) \neq j \quad \forall\ m < p < n\} \tag{69}$$

The mean of these intersample times is clearly $1/\lambda_j$ and $|\Delta k_j| = K\lambda_j$. For a given Λ, the variance of the entire sequence is the sum of the variances of the individual intersampling times to each spacecraft:

$$\sigma^2_{\text{tot}}(\bar{\boldsymbol{\mu}}) = \sum_{j \in N_i} \sigma^2(\Delta k_j) = \sum_{j \in N_i} \left[\frac{1}{K\lambda_j} \sum_{n=1}^{K\lambda_j} \left(\Delta k_j(n) - \frac{1}{\lambda_j} \right)^2 \right] \tag{70}$$

where $\Delta k_j(n)$ is the nth element in Δk_j. This quantity is easily computed for periodic sequences. Table 1 shows Δk_j and σ^2_{tot} for the three sequences.

Figure 5 illustrates the change in cost with σ^2_{tot} for sequences with varying K. Three types of sequences are considered:

1) slow switching: all measurements are grouped together, for example, $\bar{\boldsymbol{\mu}} = \{1, 1, \ldots, 2, 2, \ldots, 3, 3, \ldots\}$;

2) fast switching: the sequence which minimizes σ^2_{tot} for each K; and

3) random switching: randomly generated sequences which satisfy the duty cycles Λ.

Table 1 Intersampling times Δk_j and sequence variances σ^2, σ^2_{tot} for several measurement sequences

$\bar{\boldsymbol{\mu}}$	$\Delta k_1 = \Delta k_2$	$\sigma^2(\Delta k_1) = \sigma^2(\Delta k_2)$	$\sigma^2_{\text{tot}}(\bar{\boldsymbol{\mu}})$
$\{1, 2, 1, 2, 1, 2\}$	$\{2, 2, 2\}$	0	0
$\{1, 1, 2, 2, 1, 2\}$	$\{1, 2, 3\}$	0.67	1.33
$\{1, 1, 1, 2, 2, 2\}$	$\{1, 1, 4\}$	2	4

Although the plot shows that the mean covariance J^{FC}_∞ is not monotonically decreasing with decreasing σ^2_{tot}, the minimum cost for this case occurs when $\sigma^2_{\text{tot}} = 0$. This property has been seen in all other examples the authors have explored, including many higher order problems (i.e., larger N and K). This understanding is clearer still when considering the slow switching case (σ^2_{tot} large). In this case, as K increases only a single spacecraft is observed for an increasingly long period of time. In the limit, as K approaches infinity only a single spacecraft is observed and the information on all other spacecraft will go to zero, resulting in a high cost. Conversely, for fast switching, as K increases the cost can be made at least as small as the cost found for smaller K. Consider the optimal sequence for some fixed K, denoted by $\bar{\boldsymbol{\mu}}^*_K$. For a period length of $2K$, $3K$, etc., the sequences $\{\bar{\boldsymbol{\mu}}^*_K, \bar{\boldsymbol{\mu}}^*_K\}$, $\{\bar{\boldsymbol{\mu}}^*_K, \bar{\boldsymbol{\mu}}^*_K, \bar{\boldsymbol{\mu}}^*_K\}$, etc., will yield the same cost (as well as the same σ^2_{tot}). This places an upper bound on the cost for large K which will be lower than the cost associated with the slow switching case. Finally, for random switching, as K approaches infinity, the switching sequence approaches the random sequence found by the algorithm presented in [12].

This suggests that for systems with larger K or N, the optimal sequence may be found by minimizing σ^2_{tot}. An exhaustive search for the sequence with the minimum sampling variance would be computationally prohibitive for large K and N; however, a fast switching sequence with minimum or near-minimum sampling variance can be found in a manner similar to the integer steepest descent search algorithm described above. This method is outlined in Algorithm 3. Starting with an initial sequence $\bar{\boldsymbol{\mu}}^0_K$ the algorithm proceeds by swapping measurements for each pair of time instances $k_1, k_2 \in \{0, \ldots, K-1\}$ and evaluates the variance in Eq. (70). The sequence is updated by swapping the pair of measurements that yields the greatest decrease in variance, and the algorithm repeats until a minimum is achieved.

C. Constrained Sequence Search

The scheduling algorithm is extended to allow for a constraint on the minimum switching time of the RBS. The SS steepest descent search algorithm is modified to produce the optimal measurement

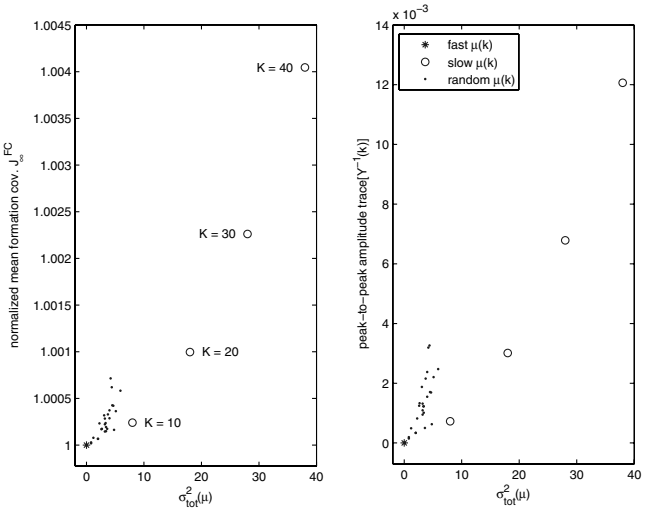

Fig. 5 Shown is the resulting formation mean covariance J^{FC} and peak-to-peak relative amplitude of trace $[\mathbf{Y}^{-1}(k)]$ for the three spacecraft system for various K where $\Lambda = \{1/2, 1/2\}$. The peak-to-peak relative amplitude is $(\max_k\{\text{trace}[\mathbf{Y}^{-1}(k)]\} - \min_k\{\text{trace}[\mathbf{Y}^{-1}(k)]\})/J^{\text{FC}}$.

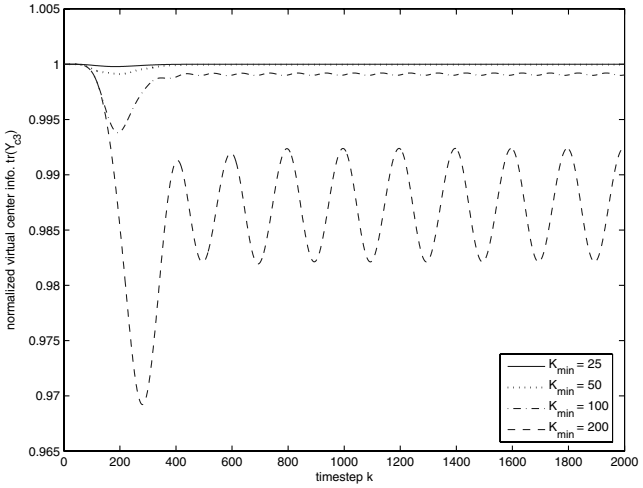

Fig. 6 Mean information decreases with increasing $K_{\min}$ and peak-to-peak amplitude increases for $K = 1000$.

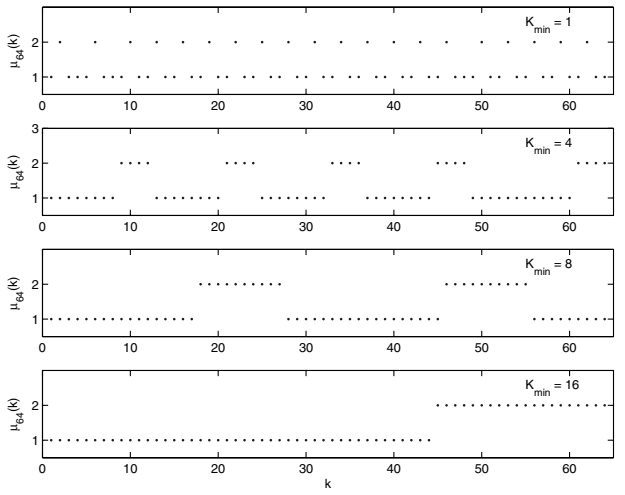

Fig. 8 Optimal measurement sequences for $K = 64$ and $K_{\min} = \{1, 4, 8, 16\}$.

schedule based on two parameters: K, the integer number of time steps in the periodic sequence, and $K_{\min}$, the minimum switching time of the sensor, also in time steps. The algorithm proceeds in the same manner as SS and DCS, with the added constraint that $\lambda_i \geq K_{\min}/K$. The implementation of the sequence generating algorithm is easily modified to account for the minimum switching time. As with the slow switching case, a decrease in performance is expected for increasing $K_{\min}$. Figure 6 shows the center state information with increasing $K_{\min}$ demonstrating this effect.

Figure 7 shows the effect of varying K and $K_{\min}$ on a modified version of the three spacecraft example. In this example, spacecraft 2 is nominally located 100 m from spacecraft 3 and remains at a bearing of $+\pi/6$ rad. Larger $K_{\min}$ requires larger K in order to achieve higher mean information. Note that λ_1^* is always within $1/K$ of the optimal λ_1 as determined by the faster DCS algorithm. Figure 8 shows the optimal measurement sequences for each $K_{\min}$ when $K = 64$.

VI. Simulation Results

An eight spacecraft 2-D simulation of a formation similar in context to the SI mission is simulated to evaluate the estimation and fuel (control) performance. The eight spacecraft are randomly placed, as shown in Fig. 9. Each spacecraft is simulated using free body dynamics with differing constant disturbance biases at each spacecraft in the range of 20–25 μN and a small random white noise component with a standard deviation of 1 μN in X^1 and X^2. Each spacecraft is equipped with 1 mN thrusters in X^1 and X^2, and each RBS provides measurements with sensor noise standard deviation of (2 cm, 1 arcsec) in range and bearing at a rate of 0.25 Hz. The controller error ellipse is defined such that $e^{(1)}_{\max} = e^{(2)}_{\max} = 1$ m and $\dot{e}^{(1)}_{\max} = \dot{e}^{(2)}_{\max} = 0$; Fig. 10 shows the effect of the control law acting on a sample spacecraft.

Table 2 shows the results of the SS algorithm for each spacecraft i on the system shown in Fig. 10 using the cost J^{CI}_{∞}. The resulting duty cycles are $\Lambda_i = \{\lambda_{ij} \mid j \in N_i\}$, $N_i = \{1, \ldots, N\} \setminus i$. The nominal ranges $\bar{R}_{ij} \triangleq \sqrt{(r^{(1)}_{ic} - r^{(1)}_{jc})^2 + (r^{(2)}_{ic} - r^{(2)}_{jc})^2}$ between each pair of spacecraft are also shown for comparison. The algorithm produces identical results for various initial guesses including those generated by the LMI solution. The results show that there is a strong correlation between ranges and the λ_{ij}. Also, the formation and center state information vary little over the period K, and it is never advantageous to not observe a spacecraft, that is, λ_{ij} is never zero. Figure 11 shows the measurement sequence and steady-state information for spacecraft 3. For the fast switching sequence shown, the information is relatively constant over the period K.

Figure 12 illustrates the effect of using the different cost functions $J^{(\cdot)}_{\infty}$ to optimize the measurement schedule at spacecraft 1. The horizontal axis represents each of the four cost functions for each of the seven spacecraft being sensed in order of decreasing range; spacecraft 2 is closest and spacecraft 3 is farthest away. Each cost function results in a measurement schedule that takes more measurements to spacecraft that are closer except J^{FC}_{∞}, which prefers

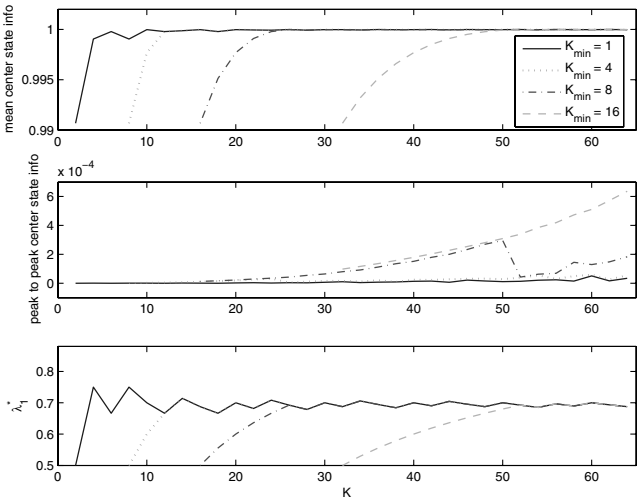

Fig. 7 Effects of small K and $K_{\min}$ using the SS algorithm with fast switching on the modified three spacecraft example.

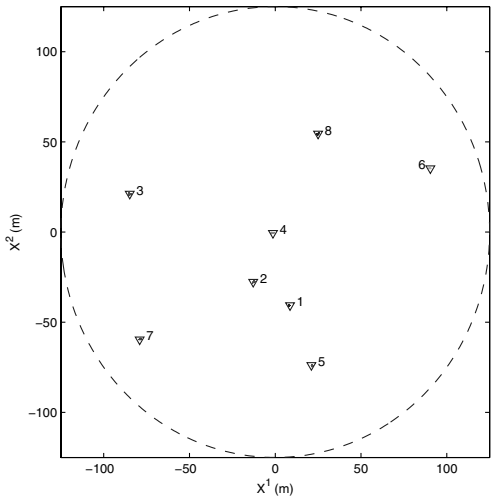

Fig. 9 Eight spacecraft 250 m baseline formation.

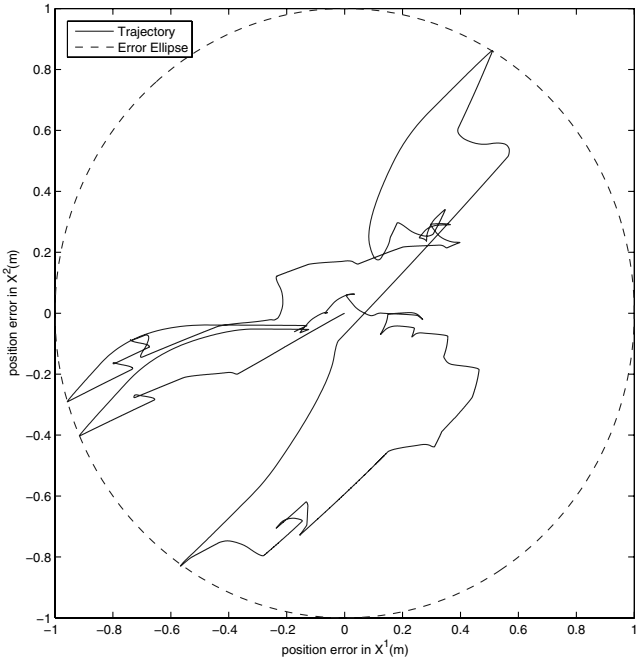

Fig. 10 Spacecraft 8 position error and controller error ellipse.

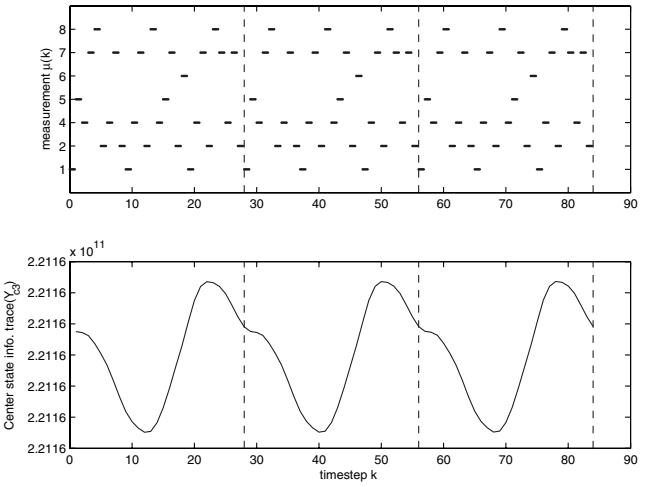

Fig. 11 Top: Optimal measurement sequence at spacecraft 3; each horizontal tick represents a single measurement. Note that the sampling sequences to each sensor are nearly uniform. Bottom: The peak-to-peak amplitude of the resulting periodic information is several orders of magnitude less than the mean [due to fast switching, i.e., low $\sigma^2_{\text{tot}}(\bar{\mu})$].

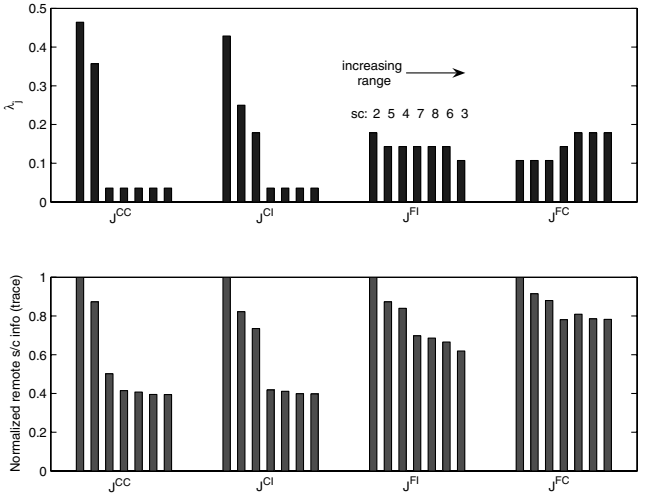

Fig. 12 Optimal Λ and resulting information at spacecraft 1. The optimal Λ when using J^{FC} resulting in higher λ_j for spacecraft that are farther away whereas the other cost functions favor close spacecraft.

spacecraft that are farther away. Of the three that prefer closer spacecraft, J^{CC} has the largest variation of the duty cycle λ_j, that is, highest lambda for spacecraft 2 and smallest for spacecraft 3; and J^{FI}_{∞} has the smallest variation. Figure 12 (bottom) represents the resulting information on each individual spacecraft normalized by the maximum (i.e., each group of seven is normalized by its max). The information resulting from the cost function J^{FC}_{∞} shows the least variation while the information resulting from J^{CC}_{∞} shows the most variation in information. This suggests that minimizing J^{FC} attempts to balance information throughout the formation.

In a final study, the distributed virtual center and sensor scheduling concepts are brought together in one comparison. All eight spacecraft are simulated, and several cases are tested:

$n > 1$ *Unweighted*: Each spacecraft is equipped with n range/bearing sensors that run concurrently and provide measurements to n spacecraft. Each sensor provides range/bearing measurements to a single remote spacecraft throughout the simulation. To balance the network and ensure coupling, each spacecraft is sensed by exactly n spacecraft. The weights $W_i = I$ in the virtual center calculations. The sensor architecture is static, that is, the RBSs do not switch between multiple remote spacecraft.

$n > 1$ *Weighted*: Identical to the $n > 1$ unweighted case except $W_i = \text{diag}(G_i, \mathbf{Y}_i)$ when calculating the virtual center and $g_i = 5$.

Switched unweighted (SU): Each spacecraft is equipped with a single RBS and the infinite horizon scheduling algorithm described in Sec. IV is used. The weighting matrix $W_i = I$ when calculating the virtual center. Three different switching sequences are used: those determined by minimizing J^{CI}_{∞}, J^{FI}_{∞}, and J^{FC}_{∞} are denoted by SUCI, SUFI, and SUFC, respectively.

Switched weighted (SI): Same as SU except the weighting matrix is $W_i = \mathbf{Y}_i$ when calculating the virtual center.

Table 2 Nominal range $\bar{R}_{ij}$ and corresponding λ_{ij} for $K = 28$

	$\bar{R}_{ij}$, m								$\lambda_{ij}K$							
i/j	1	2	3	4	5	6	7	8	1	2	3	4	5	6	7	8
1	——	25	112	41	35	112	90	97	——	12	1	5	7	1	1	1
2	25	——	87	29	57	121	74	90	12	——	1	10	2	1	1	1
3	112	87	——	86	142	176	81	115	3	6	——	6	2	1	7	3
4	41	29	86	——	77	99	98	61	7	13	1	——	2	1	1	3
5	35	57	142	77	——	129	101	128	14	6	1	3	——	1	2	1
6	112	121	176	99	129	——	194	68	4	3	2	5	3	——	1	10
7	90	74	81	98	101	194	——	154	4	7	6	4	4	1	——	2
8	97	90	115	61	128	68	154	——	3	4	2	9	2	7	1	——

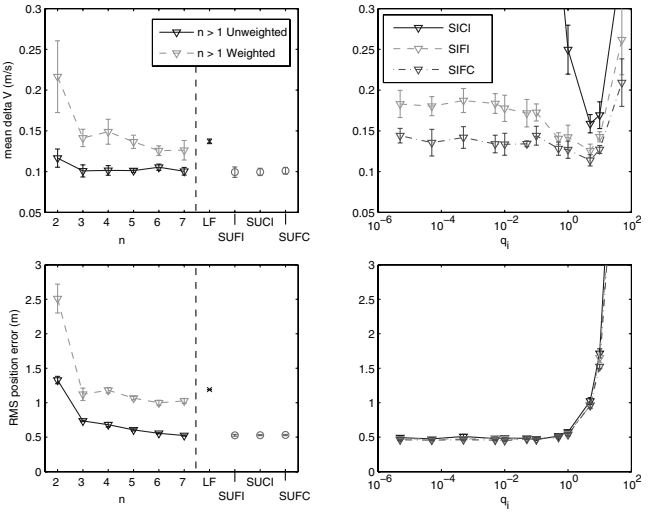

Fig. 13 Simulation of distributed unweighted ($W_i = I$) and information weighted ($W_i = \mathbf{diag}(G_i, Y_i)$) virtual center for spacecraft equipped with $n \in \{2, \ldots, 7\}$ range/bearing sensors. Traditional leader follower (1 leader, 7 followers) and switched RBS ($n = 1$) are also compared.

Leader follower (LF): Unweighted virtual center where each spacecraft maintains an estimate to spacecraft 1 only. Spacecraft 1 performs no correction maneuvers.

For each case, multiple 48 h simulations are performed. Figure 13 shows the mean fuel usage and rms position error for each case with 1-σ error bars. Note that the $n > 1$ cases are unrealistic because they require more than one RBS, but are presented here for comparison purposes only. The results show that the switched network exhibits positioning performance superior in almost every case to the LF network, and superior even to the $n > 1$ solutions. Results suggest that the switched network with a single sensor is equivalent in performance to a nearly centralized ($n = 7$) static sensor schedule solution. Also, there is a tradeoff between the robustness of the information weighted virtual center versus the performance of the unweighted weighted virtual center. The information weighted virtual center should therefore be used if failures in the estimation and sensing subsystems have a higher probability to allow for an accurate and stable estimate of the virtual center. Finally, it is noted that tuning g_i results in greatly improved performance for all information weighted cases.

VII. Conclusions

The information weighted virtual center algorithm combined with the sensor switching algorithm has been presented. The algorithm is highly decentralized, requiring only the low bandwidth transmission of maneuvers, scalable and naturally mitigates errors in the estimation/sensor subsystem. These errors may be due to unobservability of spacecraft due to the limited field of view of the RBS and occlusions, loss of lock at the RBS, and changes in the measurement and process noise covariances. The assumption that the RBS sensor provides omnidirectional measurements can be relaxed by having the spacecraft select measurements based on a reduced set of available measurements. The periodic scheduling algorithm has been shown to be convex under mild assumptions and the LMI-based approximate solution can be used in the more accurate steepest descent search algorithm. Limitations in sensor switching frequency are incorporated by adding the appropriate constraints in the steepest descent search scheduling algorithm. Simulation results show the decentralized information weighted virtual center calculation coupled with optimal sensor scheduling to yield performance (estimation, fuel usage, and positioning) that is superior to leader follower using a single RBS sensor and comparable to a fully connected architecture where each spacecraft is equipped with $N - 1$ range/bearing sensors.

References

[1] Windt, D., Kahn, S., and Sommargen, G., "Diffraction-Limited Astronomical X-Ray Imaging and X-Ray Interferometry Using Normal-Incidence Multilayer Optics," *Proceedings of SPIE*, Vol. 4851, March 2003, pp. 441–450.

[2] Beichman, C., Coulter, D., Lindensmith, C., and Lawson, P., "Summary Report on Architecture Studies for the Terrestrial Planet Finder," JPL Publ. 02-011, June 2002.

[3] Carpenter, K. G., Schrijver, C. J., Lyon, R. G., Mundy, L. G., Allen, R. J., Armstrong, J. T., Danchi, W. C., Karovska, M., Marzouk, J., Mazzuca, L. M., Mozurkewich, D., Neff, S. G., Pauls, T. A., Rajagopal, J., Solyar, G., and Zhang, X., "The Stellar Imager (SI) Mission Concept," *Proceedings of SPIE*, Vol. 4854, Feb. 2003, pp. 293–302.

[4] Aung, M., Purcell, G., Tien, J., Young, L., Amari, L., Srnvasan, J., Ciminera, M., and Chong, Y., "Autonomous Formation-Flying Sensor for the StarLight Mission," IPN Progress Rept. 42-152, JPL, Feb. 2003.

[5] Hadaegh, F., Scharf, D., and Ploen, S., "Initialization of Distributed Spacecraft for Precision Formation Flying," *Proceedings of the IEEE Conference on Control Applications*, Vol. 1, IEEE, New York, June 2003.

[6] Scharf, D., Hadaegh, F., and Ploen, S., "A Survey of Spacecraft Formation Flying Guidance and Control (Part 2): Control," *American Control Conference, Proceedings of the IEEE*, Vol. 4, IEEE, New York, 2004, pp. 2976–2985.

[7] Tillerson, M., Breger, L., and How, J., "Distributed Coordination and Control of Formation Flying Spacecraft," *Proceedings of the IEEE American Control Conference*, IEEE, New York, June 2003.

[8] Carpenter, J., "Decentralized Control of Satellite Formations," *International Journal of Robust and Nonlinear Control*, Vol. 12, No. 2, Feb. 2002, pp. 141–161.

[9] Campbell, M., "Planning Algorithm for Multiple Satellite Clusters," *Journal of Guidance, Control, and Dynamics*, Vol. 26, No. 5, 2003, pp. 770–780.

[10] Meier, L., Peschon, J., and Dressler, R., "Optimal Control of Measurement Systems," *IEEE Transations on Automatic Control*, Vol. AC-12, No. 5, Oct. 1967, pp. 528–536.

[11] Savkin, A., Evans, R., and Skafidas, E., "The Problem Of Optimal Robust Sensor Scheduling," *Proceedings of the IEEE Conference on Decision and Control*, Vol. 4, IEEE, New York, Dec. 2000, pp. 3791–3796.

[12] Gupta, V., Chung, T., Hassibi, B., and Murray, R., "Sensor Scheduling Algorithms Requiring Limited Computation," *International Conference on Acoustics, Speech, and Signal Processing* (submitted for publication).

[13] Feron, E., and Olivier, C., "Targets, Sensors and Infinite-Horizon Tracking Optimality," *Proceedings of the 29th IEEE Conference on Decision and Control*, Vol. 4, IEEE, Wahington, D.C., Dec. 1990, pp. 2291–2292.

[14] Scharf, D., Hadaegh, F., and Kang, B., "On the Validity of the Double Integrator Approximation in Deep Space Formation Flying," *International Symposium on Formation Flying Missions & Technologies*, NASA Center for Aerospace Information, Hanover, MD, 2002.

[15] Miller, I., and Campbell, M., "Validation of Simplified Formation Models at L2," *Proceedings of the IEEE American Control Conference*, IEEE, New York, June 2005.

[16] Mutambara, A., *Decentralized Estimation and Control for Multisensor Systems*, CRC Press, Boca Raton, FL, 1998.

[17] Bittanti, S., Colaneri, P., and Nicolao, G. D., "The Periodic Riccati Equation," *The Riccati Equation*, edited by S. Bittanti, A. Laub, and J. Willems, Springer–Verlag, New York, 1991, pp. 127–162.